Title: Dopant Binding with Vacancies and Helium in Metal Hydrides

Authors: Amy Kaczmarowski[a,b], Clark Snow[a], Stephen Foiles[a], Corbett Battaile[a], Dane Morgan[b]

[a] Sandia National Laboratories, Albuquerque, New Mexico, USA, corresponding author:akaczma@sandia.gov

[b] Department of Materials Science and Engineering, University of Wisconsin-Madison, Madison, Wisconsin, USA

Abstract

Metal hydrides are crucial for the long-term storage of tritium but suffer degradation due to the buildup and release of helium decay products. Therefore, it is of interest to explore how dopants in these metal hydrides may impact helium bubble nucleation and distributions, as well as associated fracture and helium retention. Prior studies have focused on helium behavior in pure metal hydrides or with one or two types of impurities. Analytical models have also shown that the concentration of nucleated bubbles can impact the time to fracture of materials. This study utilizes high-throughput density functional theory calculations to identify the impact of transition metal substitutional dopants on helium binding energies in face-centered cubic metal hydrides, such as erbium hydride, holmium hydride, scandium hydride, titanium hydride, yttrium hydride, and zirconium hydride. This study also explores the impact of hydrogen vacancies on the binding energy of helium near the substitutional defects. Finally, this study presents an initial assessment of dopant stability and solubility limits at many temperatures and pressures. Several metals strongly bind to helium in these metal hydrides, making them promising for influencing helium nucleation and subsequent bubble growth. However, many of these potentially beneficial substitutional defects have low solubility limits. The calculations show that some strong binding dopants may be soluble in quantities that affect the bubble concentration and impact material performance.

Highlights:

- High throughput calculations of dopants in FCC metal hydrides
- Calculations of dopant binding with hydrogen vacancies and helium interstitials
- Implications for helium bubble nucleation

Keywords:

Metal Hydride, Helium, Erbium, Holmium, Scandium, Titanium, Yttrium, Zirconium, Tritium, Transition Metals.

1. Introduction

A variety of applications utilize metal hydrides such as switchable mirrors [1][2][3][4], sensors [5][6][7], and the storage of hydrogen and its isotopes for energy production [8][9][10][11][12][13]. Metal hydrides provide a stable means to store high densities of hydrogen for long periods. While many different metals can form metal hydrides, some metals are more useful than others for specific applications. Erbium hydride, holmium hydride, scandium hydride, titanium hydride, yttrium hydride, and zirconium hydride [14] are among the common metal hydrides used to store tritium for fusion applications.

Storage of tritium, especially for long periods, can prove problematic for metal hydrides due to their brittle nature and the buildup of helium. Tritium is a radioactive isotope of hydrogen and undergoes beta decay with a half-life of approximately 12.32 years. Equation 1 shows this decay mode.

$$ {}_1^3T \rightarrow {}_2^3He^{1+} + e^- + \bar{\upsilon_e} \qquad 1 \text{ [15]} $$

The decay of tritium to helium in metal hydrides eventually leads to helium bubble formation, which generates stresses in the metal hydride and impairs its performance over time. While nucleation of helium bubbles from tritium decay in metal hydrides can occur quickly (~1 month), it can often take several years for helium to accumulate in sufficient quantities to cause fracture of the metal hydride storage materials [16]. Nonetheless, this helium-driven fracture mode presents a significant problem for long-term storage of tritium in metal hydrides. Altering the nucleation and growth of helium bubbles in these metal hydrides may help extend the storage times for tritium.

Metals in radioactive environments have similar challenges with the growth of gas bubbles and often experience property degradation and material failure as a result. In these applications, microstructural alterations impact the accumulation and release of noble gases [17][18][19][20][21].

This paper will review the role of dopants and vacancies on the binding energy of helium and discuss the potential for using targeted dopants to control the distribution and growth of helium bubbles in metal hydrides.

2. Methods

To understand the impact of dopants on the distribution and growth of helium in metal hydrides, we evaluated various types of helium point defects in several metal hydrides. We (1) identified the helium defects that were most stable in metal hydrides as these are likely to represent the early stages of helium bubble nucleation. Then we reviewed their interaction with a metal substitutional dopant. We (2) identified those substitutional dopants that bound most strongly with these defects as they would likely act as trapping sites and impact the He bubble nucleation, growth and eventually impact the material properties and performance. Finally, we examined the stability of these dopants in the metal hydrides. We (3) analyzed those dopants that could be introduced at high enough concentrations to impact helium distribution without forming competing phases in the metal hydrides. This section describes the specifics of these calculations. Ideally, the calculations would be carried out on a range of realistic He bubble structures from many stages of nucleation, growth, and coarsening to provide the best guidance of their potential impact on the He bubble microstructure evolution. However, due to the enormous complexity of such studies, the present work treated only single He interstitial binding to dopants and vacancies. Under the hypothesis that trends from these limited sets of calculations will continue to hold for larger clusters, these trends guide how dopants impact the growth and formation of helium bubbles. However, this hypothesis is still speculative and needs additional study in future work.

While there are many different types of transition metal and rare-earth metal hydrides, we focused on metals with the calcium fluoride metal di-hydride structure shown in Figure 1. The metal atoms form a face-centered cubic (FCC) structure, with the hydrogen atoms filling the tetrahedral sites. Specifically, we consider erbium hydride (ErH_2), holmium hydride (HoH_2), scandium hydride (ScH_2), titanium hydride (TiH_2), yttrium hydride (YH_2), and zirconium hydride (ZrH_2), all systems of interest for long term tritium storage.

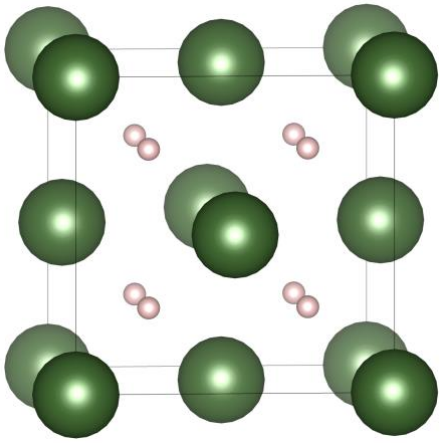

Figure 1. FCC metal di-hydride structure. The large green features represent the metal atom sites and small pink features represent the hydrogen sites.

The properties of these systems were determined using density functional theory calculations with the Vienna ab initio simulation package (VASP) v5.3.5 [22]. The generalized gradient approximation was used for the exchange and correlation energy functionals with the Perdew Burkee Ernzerhof functional (PBE)[23]. The calculations were performed with spin polarization. The PAW[24] potentials used in this study are listed in Table 1. An energy cutoff of 600 eV and a Monkhorst-Pack k-point grid density of 10×10×10 (for a 2×2×2 cell, with 32 MH_2 formula units) were used. See section one of the supplemental to this paper for more details on the convergence of each system.

Table 1. VASP PAW potentials used for calculations

Metal	Pseudopotential	Metal	Pseudopotential
Au	Au ($5d^{10}6s^1$)	**Ni**	Ni_pv ($3p^63d^84s^2$)
Ag	Ag ($4d^{10}5s^1$)	**Os**	Os_pv ($5p^65d^66s^2$)
Cd	Cd ($4d^{10}5s^2$)	**Pd**	Pd ($4d^{10}$)
Co	Co ($3d^74s^2$)	**Pt**	Pt ($5d^96s^1$)
Cr	Cr_pv ($3p^63d^54s^1$)	**Re**	Re_pv ($5p^65d^56s^2$)
Cu	Cu_pv ($3p^63d^{10}4s^1$)	**Rh**	Rh_pv ($4p^64d^8s^1$)
Er	Er_3 ($4f^16s^2$)	**Ru**	Ru_pv ($4p^64d^75s^1$)
Fe	Fe_pv($3p^63d^64s^2$)	**Sc**	Sc_sv ($3s^23p^63d^14s^2$)
H	H ($1s^1$)	**Ta**	Ta_pv ($5p^65d^36s^2$)
He	He ($1s^2$)	**Ti**	Ti_pv ($3p^63d^24s^2$)
Hf	Hf_pv ($5p^65d^26s^2$)	**V**	V_sv ($3s^23p^63d^34s^2$)

Ho	Ho_3 ($4f^{1}6s^{2}$)	**W**	W_pv ($5p^{6}5d^{4}6s^{2}$)
Ir	Ir ($5d^{7}6s^{2}$)	**Y**	Y_sv ($4s^{2}4p^{6}4d^{1}5s^{2}$)
Mn	Mn_pv ($3p^{6}3d^{5}4s^{2}$)	**Zn**	Zn ($3d^{10}4s^{1}$)
Mo	Mo_pv ($4p^{6}4d^{5}5s^{2}$)	**Zr**	Zr_sv ($4s^{2}4p^{6}4d^{2}5s^{2}$)
Nb	Nb_pv ($4p^{6}4d^{4}5s^{1}$)		

We used these parameters to calculate the lattice constants for the pure metal hydride systems and found a good agreement between our results and experimental and calculated literature values. Table 2 shows a comparison of these values. Experiments have identified that TiH_2 and ZrH_2 form stable face centered tetragonal (FCT) structures at lower temperatures [25]. These FCT structures were not considered further but are shown here to compare to the FCC structures used in this study.

Table 2. Metal hydride lattice constants calculated compared to literature and experimental values

Metal Hydride	Lattice Parameters				
	Calculated (this work)	DFT Literature	Percent Error	Experimental Literature	Percent Error
ErH_2	5.123	5.129[a]	0.117	5.126[c]	0.0585
HoH_2	5.1611	5.1611	0	5.165[d]	0.078
ScH_2	4.777	4.740[b]	-0.781	4.78[e]	0.0628
TiH_2 (FCC)	4.42	4.3986[b]	-0.580	4.460 ($TiH_{1.95}$)[f]	0.804
TiH_2 (FCT)	a = 4.542 c = 4.179	a = 4.513[b] c = 4.179[b]	a = -0.643 c = 0	a = 4.528[g] c = 4.279[g]	a = -0.3092 c = 2.337
YH_2	5.204	5.2001[b]	-0.075	5.2032[h]	-0.0154
ZrH_2 (FCC)	4.815	4.804[b]	-0.229	4.780 ($ZrH_{1.55}$)[f]	-0.7322
ZrH_2 (FCT)	a = 5.007 c =4.406	a = 5.008[b] c = 4.419[b]	a = 0.02 c = 0.294	a = 4.975[i] c = 4.447[i]	a = -0.6432 c = 0.9220

[a] Schultz and Snow[14]
[b]W. Wolf and P. Herzig[26]
[c]Grimshaw et. al[27]
[d]Pebler and Wallace[28]
[e]Khodryev and Baranova[29]
[f]Ducastelle et. al.[25]
[g]Yakel[30]
[h]Daou and Vajda[31]
[i]Niedzwiedz et. al.[32]

We next evaluated the behavior of helium point defects in metal hydrides to understand which sites are stable and may lead to the nucleation of helium bubbles. In addition to those sites explored in previous studies, we utilized a large-scale search algorithm based on the metal

hydride Wyckoff positions and symmetry to identify internal spaces with sufficient volume to serve as potential locations of helium interstitial defects and dumbbells. For the metal hydride systems considered in this study without any hydrogen vacancies, the most stable structure is one with helium on the octahedral site (Figure 2A). When a tetrahedral hydrogen vacancy is present, the helium atom prefers to sit in the tetrahedral site rather than the octahedral site (Figure 2B). Several past studies have analyzed helium and hydrogen behavior in these metal hydrides [34][35][36], and we refer the reader to these studies for a more detailed analysis of these interactions. The placement of helium in the presence of hydrogen interstitials and vacancies identified in this study is consistent with past computational studies [34]. Section 2 and section 3 of the supplemental information provide details of this defect computation. We explored helium defects in a perfect metal hydride lattice and those near a hydrogen vacancy because both may occur in real systems. Hydrogen vacancy defects can be produced from low hydrogen content during the loading of the metal hydride or from the decay of tritium into helium. Helium defects surrounded by a perfect lattice may also occur because the helium has some initial energy (~0.35eV) when generated (as shown in equation 1), allowing the helium to migrate away from the hydrogen vacancy and act as a lone interstitial.

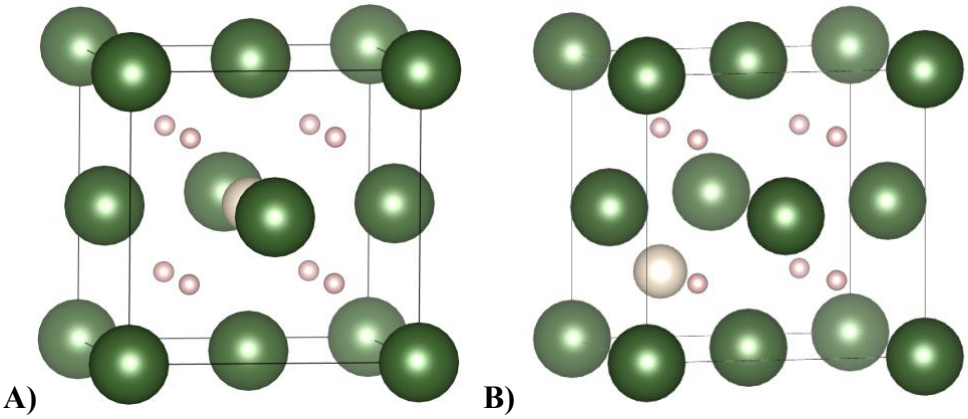

Figure 2. Stable interstitial helium sites. Green atoms represent the nominal metal of the metal hydride, the small pink atoms represent the hydrogen, and the large white atoms represent the helium. A) Helium in octahedral position with hydrogen in tetrahedral positions. B) Helium in tetrahedral site.

To evaluate the role of substitutional dopants on the nucleation and growth of helium bubbles in metal hydrides, we determined the impact of these dopants on the formation energy and binding

energy of helium interstitials and hydrogen vacancies. Figure 3 shows the structures of the substitutional defects considered in this study.

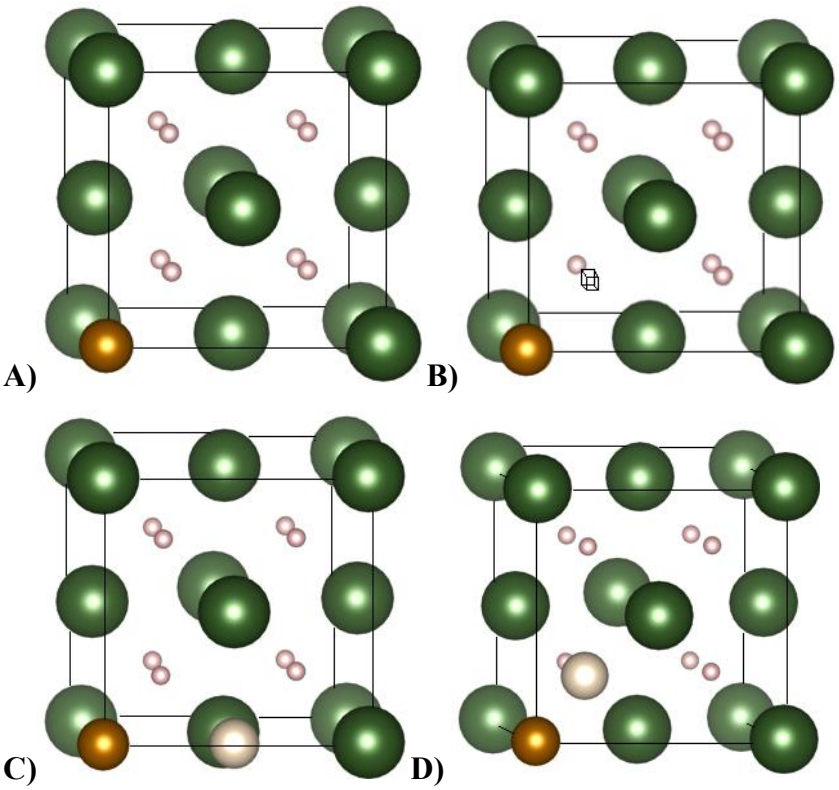

Figure 3. Substitutional defect structures. Green atoms represent the nominal metal of the metal hydride, the brown atom represents the substitutional dopant, the small pink atoms represent the hydrogen, and the large white atoms represent the helium. A) Substitutional dopant in perfect metal hydride. B) Substitutional dopant with hydrogen vacancy shown as empty cube. C) Substitutional dopant with helium octahedral interstitial. D) Substitutional dopant with hydrogen vacancy and substitutional helium on the hydrogen sublattice (tetrahedral site). Note the actual computational cell size was 2×2×2.

We generated the dopant structures for this study by substituting one of the metal atoms in the metal hydride with a new transition metal. This study focused on the use of the transition metals listed in Table 1 as substitutional defects. The formation energy of such a substitutional structure, as shown in Figure 3A, is given by (2).

$$E^f_{\mathrm{Dop}} = E_{\mathrm{Dop}} - E_{\mathrm{perf}} - \mu_{\mathrm{Dop}} + \mu_{\mathrm{M}} \qquad 2$$

In this equation, E^f_{Dop} is the formation energy of the substitutional structure, E_{Dop} is the energy of the structure with a substitutional dopant, E_{perf} is the energy of the perfect metal hydride

structure, μ_{Dop} is the chemical potential of the substitutional metal, and μ_{M} is the chemical potential of the metal used in the base metal hydride. The choice of the substitutional and base metal chemical potentials used in this equation allows one to quickly approximate the stability of these substitutions relative to common pure metal reference states. For the values in this paper, we calculated the reference state using VASP with similar parameters as described in the bulk metal hydride simulations. These values agreed with published literature values for these metals. Substitutional dopant structures with lower formation energy than other dopant structures may imply that these dopants are more stable. However, more detailed calculations to determine how much dopant can be added before generating competing phases are needed to gauge the solubility of these dopants and are discussed later in this section.

The binding energy of a hydrogen vacancy to the substitutional atom, as shown in the structure in Figure 3B, is given by (3).

$$\boldsymbol{E^{B}_{\mathrm{Dop}+V_H}} = \left(\boldsymbol{E}_{\mathrm{dop}} + \boldsymbol{E}_{\mathrm{MH_2}+V_H}\right) - \left(\boldsymbol{E}_{\mathrm{Dop}+V_H} + \boldsymbol{E_{MH_2}}\right) \quad 3$$

In this equation, $E_{\mathrm{Dop+V_H}}$ is the energy of the structure with a substitutional dopant near a tetrahedral hydrogen vacancy, $E_{\mathrm{MH_2+V_H}}$ is the energy of the metal hydride structure with a hydrogen vacancy, E_{Dop} is the energy of the structure with a substitutional dopant, and $E_{\mathrm{MH_2}}$ is the energy of the perfect metal hydride structure. In this equation, a more positive binding energy indicates that the hydrogen vacancy binds more strongly to the dopant atom than the base metal in the metal hydride.

The binding energy of a helium interstitial to the substitutional atom, as shown in the structure in Figure 3C, is given by (4).

$$\boldsymbol{E^{B}_{\mathrm{Dop+He}}} = \left(\boldsymbol{E_{\mathrm{Dop}}} + \boldsymbol{E_{\mathrm{MH_2+He}}}\right) - \left(\boldsymbol{E_{\mathrm{Dop+He}}} + \boldsymbol{E_{\mathrm{MH_2}}}\right) \quad 4$$

In this equation, $\mathrm{E_{Dop+He}}$ is the energy of the structure with a substitutional dopant near a helium interstitial, $E_{\mathrm{MH_2+He}}$ is the energy of the metal hydride structure with a helium interstitial, E_{Imp} is the energy of the structure with a substitutional dopant, and $E_{\mathrm{MH_2}}$ is the energy of the perfect metal hydride structure. In this equation, a more positive binding energy indicates that the helium atom binds more strongly to the dopant atom than the base metal in the metal hydride.

The binding energy of a helium interstitial and hydrogen vacancy to the substitutional atom, as shown in the structure in Figure 3D, is given by (5).

$$\boldsymbol{E^{B}_{\mathrm{Dop+He+V_H}} = \left(E_{Dop} + E_{MH_2+He+V_H}\right) - \left(E_{Dop+He+V_H} + E_{MH_2}\right)} \quad 5$$

In this equation, $E_{\mathrm{Dop+He+V_H}}$ is the energy of the structure with a substitutional dopant near a tetrahedral helium interstitial with a hydrogen vacancy, $E_{\mathrm{MH_2+He+V_H}}$ is the energy of the metal hydride structure with a tetrahedral helium interstitial with a hydrogen vacancy, E_{Dop} is the energy of the structure with a substitutional dopant, and $E_{\mathrm{MH_2}}$ is the energy of the perfect metal hydride structure. In this equation, a more positive binding energy indicates that the helium atom and hydrogen vacancy bind more strongly to the dopant atom than the base metal in the metal hydride.

As we considered many different metal hydride systems along with various dopants and defect states, we utilized the MAterials Simulation Toolkit (MAST) to facilitate high-throughput calculations [33][37]. MAST is an open-source python-based automated workflow manager for atomistic simulations. It is freely available through the python package index. MAST enabled automated analysis of the lattice constants for the bulk metal hydride as well as formation energies of hydrogen vacancies, helium interstitials, metal atom substitutions, and combinations of these defects.

Finally, we analyzed the thermodynamics of the mixing of the dopant with the metal hydride to identify the quantity of dopant metal that could be added before competing phases would form (the solubility limit of the dopant). This analysis would determine whether those dopants that bond most strongly with the helium and hydrogen defects could impact helium bubble formation and growth. One can consider many competing phases in a ternary structure, such as a metal hydride with dopants. For the sake of simplicity, we evaluated three primary competing reaction mechanisms. The first reaction, shown in equation (6), presents the combination of the metal for the base metal hydride (M) with the metal for the dopant (D) and hydrogen to form the substitutional dopant, as shown in Figure 3A ($M_{1-n}D_nH_2$). In this equation, n represents the number of dopant atoms added in place of the base metal atom. Note that this reaction differs from the formation energy described in equation (2) as equation (2) represents the substitution of

the dopant into an existing metal hydride. In contrast, this equation identifies the creation of the substitutional dopant metal hydride from the pure metal and hydrogen states. The relevance of these two calculations depends on the formation mechanism used. We present both in this paper for completeness.

$$(1-n)M + nD + H_2 \rightarrow M_{1-n}D_nH_2 \quad (6)$$

The second reaction, shown in equation (7), presents the combination of the metal for the base metal hydride (M) with the metal for the dopant (D) and hydrogen to form the primary metal hydride and a competing dopant metal di-hydride phase (DH2).

$$(1-n)M + nD + H_2 \rightarrow (1-n)MH_2 + nDH_2 \quad (7)$$

The third reaction, shown in equation (8), presents the combination of the metal for the base metal hydride (M) with the metal for the dopant (D) and hydrogen to form the primary metal hydride and a competing dopant metal mono-hydride phase (DH).

$$(1-n)M + nD + \left(1-\frac{n}{2}\right)H_2 \rightarrow (1-n)MH_2 + nDH \quad (8)$$

To summarize, the reactions (6), (7), and (8) correspond to the dopant metal entering the hydride as a substitutional dopant, forming a dihydride, or forming a monohydride, respectively. In addition to the metal and metal hydride phases described in these reactions, many different types of complex intermetallic phases (M_xD_y phases) can form. Often these intermetallic phases are significantly more stable than the separated metal hydride phases considered in these equations. Because these calculations neglect these intermetallic phases, our solubility limits represent extreme upper bounds, as lower solubility could result from the inclusion of more dopant hydride phases in the analysis. This simplification allows researchers to quickly compare the large variety of transition metal atoms chosen in this study. Subsequent comparisons to the various intermetallic competing phases should be performed for those metals that show the most promise, but this is beyond the scope of the present work.

To identify the solubility limit of the dopant atom as a substitutional atom in the base metal hydride, we calculate the amount of dopant atom (denoted by *n*, which is the number of moles of dissolved dopant per mole H_2 in the hydride) such that the Gibbs free energy difference (ΔG) between the substitutional reaction (Eq. (6)) and the competing reactions (Eqs. (7), (8)) is equal to zero which we write using the following conditions (where $\Delta G^{MDH2-DH2}$ and $\Delta G^{MDH2-DH}$ represent the free energy differences between Eq. (6) and Eqs. (7), or the substitutional dopant

and dopant di-hydride phases, and between Eq. (6) and (8), or the substitutional dopant and dopant mono-hydride phases, respectively):

$$\Delta G^{MDH_2-DH_2} = 0$$
$$\Delta G^{MDH_2-DH} = 0 \quad 9$$

A few additional assumptions are made to solve for the Gibbs free energy of formation of these reactions. We assumed that the pressure and volume contributions of the solids are small compared to the contribution from the hydrogen gas. This allows the solid phase PV terms in the Gibbs energy to be neglected. We also assumed that the vibrational contributions to the entropy (S_{vib}) and energy (U_{vib}) of the metal hydrides and mixtures are a sum of their components. Specifically, we assume that the vibrational entropy of a metal hydride is equal to the vibrational entropy of the metal atoms in the metal hydride plus the vibrational entropy of the hydrogen atoms in the metal hydride. In other words, the following equations are assumed to be approximately true:

$$U_{\mathrm{vib}}^{\mathrm{M_{1-n}D_nH_2}} \approx (1-n)U_{\mathrm{vib}}^{\mathrm{M}} + nU_{\mathrm{vib}}^{\mathrm{D}} + U_{\mathrm{vib}}^{\mathrm{H_2}} \quad 10$$
$$S_{\mathrm{vib}}^{\mathrm{M_{1-n}D_nH_2}} \approx (1-n)S_{\mathrm{vib}}^{\mathrm{M}} + nS_{\mathrm{vib}}^{\mathrm{D}} + S_{\mathrm{vib}}^{\mathrm{H_2}} \quad 11$$
$$U_{\mathrm{vib}}^{\mathrm{DH_2}} \approx U_{\mathrm{vib}}^{\mathrm{D}} + U_{\mathrm{vib}}^{\mathrm{H_2}} \quad 12$$
$$S_{\mathrm{vib}}^{\mathrm{DH_2}} \approx S_{\mathrm{vib}}^{\mathrm{D}} + S_{\mathrm{vib}}^{\mathrm{H_2}} \quad 13$$

This assumption allows us to argue that the vibrational entropy/enthalpy of component atoms (M, D, H) in one structure are approximately equal to the vibrational entropy/enthalpy in a different structure. This assumption is more valid for the dopant di-hydride case ($\Delta G^{MDH_2-DH_2}$) because the $M_{1-n}D_nH_2$, MH_2, and DH_2 structures are very similar. Therefore, the metal atoms, dopant atoms, and hydrogen atoms likely have similar vibrational entropy/enthalpy across the structures. For the dopant mono-hydride case, we assume that the dopant atoms in the DH structure will have similar vibrational entropy/enthalpy to dopant atoms in the $M_{1-n}D_nH_2$. If n is small we believe that this assumption is acceptable.

We also assumed that the substitutional hydride mixture acts as an ideal mixture. Therefore the following equation is assumed to be approximately true.

$$S_{\mathrm{Config}}^{\mathrm{M_{1-n}D_nH_2}} = \frac{1}{2}k[nln(n) + (1-n)ln(1-n)] \quad 14$$

where S represents the entropy of the mixture and k is the Boltzmann constant. The energy of the dopant metal hydride as a function of n can be approximated by:

$$E_{\mathrm{VASP}}^{\mathrm{MDH_2}}(n) = n\left(E_{\mathrm{VASP}}^{\mathrm{M_{31}D_1H_{64}}} - E_{\mathrm{VASP}}^{\mathrm{MH_2}}\right) + E_{\mathrm{VASP}}^{\mathrm{MH_2}} \quad 15$$

In this equation, E_{VASP} represents the configurational energy calculated by VASP.

While these simplifications allow the hydrogen vibrational terms in the competing dopant di-hydride case to cancel with those in the substitutional metal hydride case, there are remaining hydrogen terms in the dopant mono-hydride case to be considered. An Einstein vibrational model is assumed to calculate the vibrational contribution to the entropy and energy of hydrogen in the solid. The Einstein temperatures (Θ_E) for H in the metal di-hydrides and mono-hydrides are determined from the optical peak frequencies measured by scattering cross-section of hydrogen in [38] for various metal hydrides. From these calculations, average Einstein temperatures for the hydrogen in the metal mono-hydride was approximately 1070K and approximately 1525K for the metal-dihydrides. While these values may not encompass every potential structure, the contribution from variations in these Einstein temperatures is small. This model leads to the following equations for the vibrational contribution to the entropy and energy of hydrogen in the solid, where T is the temperature in Kelvin.

$$U_{\mathrm{vib}}^{\mathrm{H_2\ or\ H}} = 3kTln\left[2\sinh\left(\frac{\Theta_E}{2T}\right)\right] \quad 16$$

$$S_{\mathrm{vib}}^{\mathrm{H_2\ or\ H}} = 3k\frac{\Theta_E}{2T_0}\coth\left(\frac{\Theta_E}{2T_0}\right) \quad 17$$

The NIST thermodynamic database was used to calculate the Gibbs free energy of formation of the pure hydrogen gas [39] as shown in the following equation where P is the partial pressure of H and P_0 is 1 atm.

$$G_f^{H_2}(T,P) = E_{\mathrm{VASP}}^{\mathrm{H_2}} - \left(H_{\mathrm{NIST}}^{\mathrm{H_2}}(T=0,P_0) - H_{\mathrm{NIST}}^{\mathrm{H_2}}(T=T,P_0)\right) + kTln\left(\frac{P}{P_0}\right) - TS_{\mathrm{NIST}}^{\mathrm{H_2}}(T) \quad 18$$

Applying these simplifying assumptions to the Gibbs reaction equations leads to the result below. We provide additional details leading to these equations in section 5 of the supplemental material.

$$\Delta G^{MDH_2-DH_2} = nE_{\mathrm{VASP}}^{\mathrm{MDH_2}} - TS_{\mathrm{Config}}^{\mathrm{MDH_2}} - nE_{\mathrm{VASP}}^{\mathrm{DH_2}} \quad 19$$

$$\Delta G^{MDH_2-DH} = n\left[E_{\mathrm{VASP}}^{\mathrm{MDH_2}} + U_{\mathrm{vib}}^{\mathrm{H_2}} - TS_{\mathrm{vib}}^{\mathrm{H_2}} - E_{\mathrm{VASP}}^{\mathrm{DH_2}} - U_{\mathrm{vib}}^{\mathrm{H}} + TS_{\mathrm{vib}}^{\mathrm{H}} - \frac{1}{2}G_f^{\mathrm{H_2}}\right] - TS_{\mathrm{Config}}^{\mathrm{MDH_2}} \quad 20$$

These equations can be evaluated at various hydrogen partial pressures and temperatures to identify the relative stability of the substitutional phase compared to the competing metal and metal hydride phases. It should be noted that the hydrogen partial pressure will only impact the

metal phase and dopant mono-hydride phase as the pressure-dependent terms cancel in ΔG^{MDH_2-DH}.

3. Results

A. Dopants in metal hydrides

The formation energy of the substitutional defects as determined by (2) with different reference states used for the chemical potentials are shown in Figure 4. This figure demonstrates that the formation energy for these substitutional defects can be quite large and depends quite significantly on the choice of reference state. While these plots provide some indication of which substitutions will be more likely to occur, it is difficult to identify how much of a given substitution can be created in a metal hydride before a competing phase occurs. The results in section E provide a more detailed look at the actual solubility of the dopants.

A)

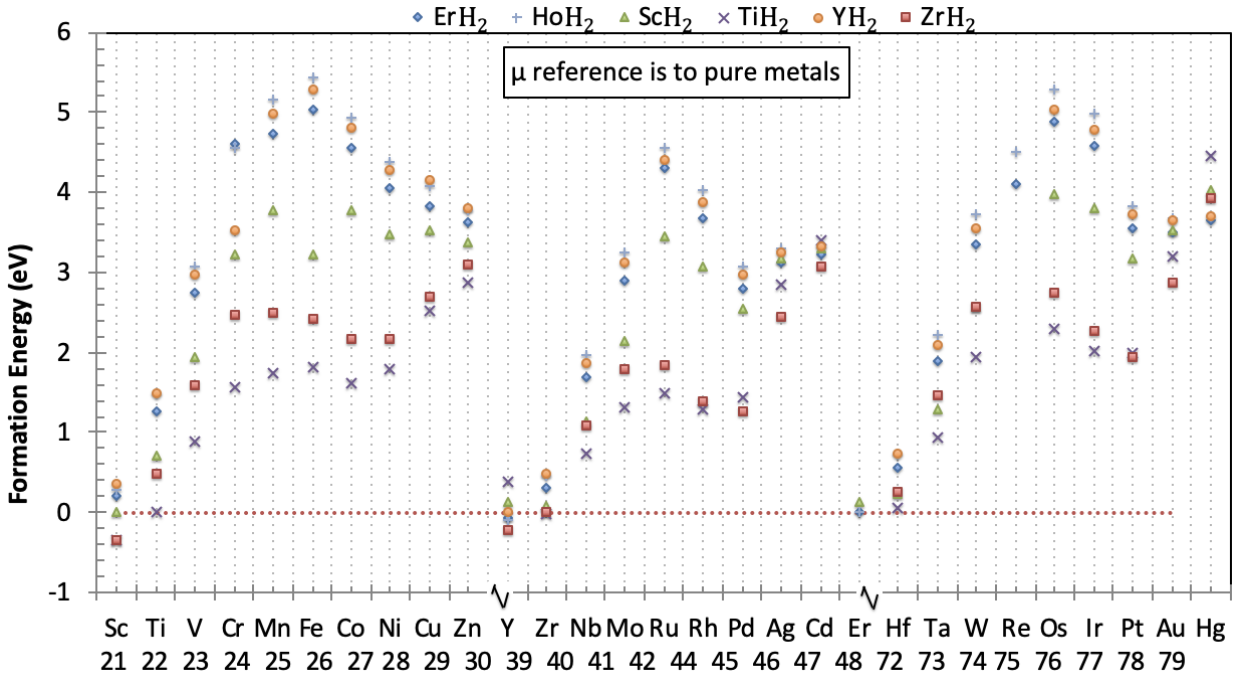

B)

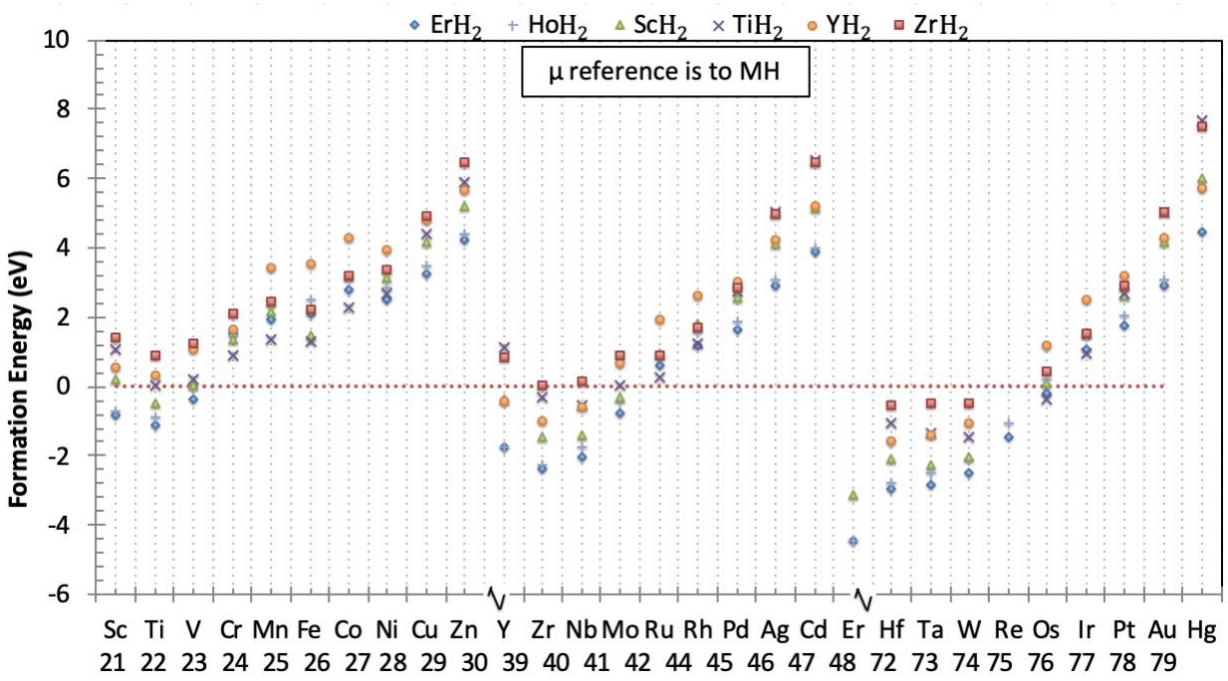

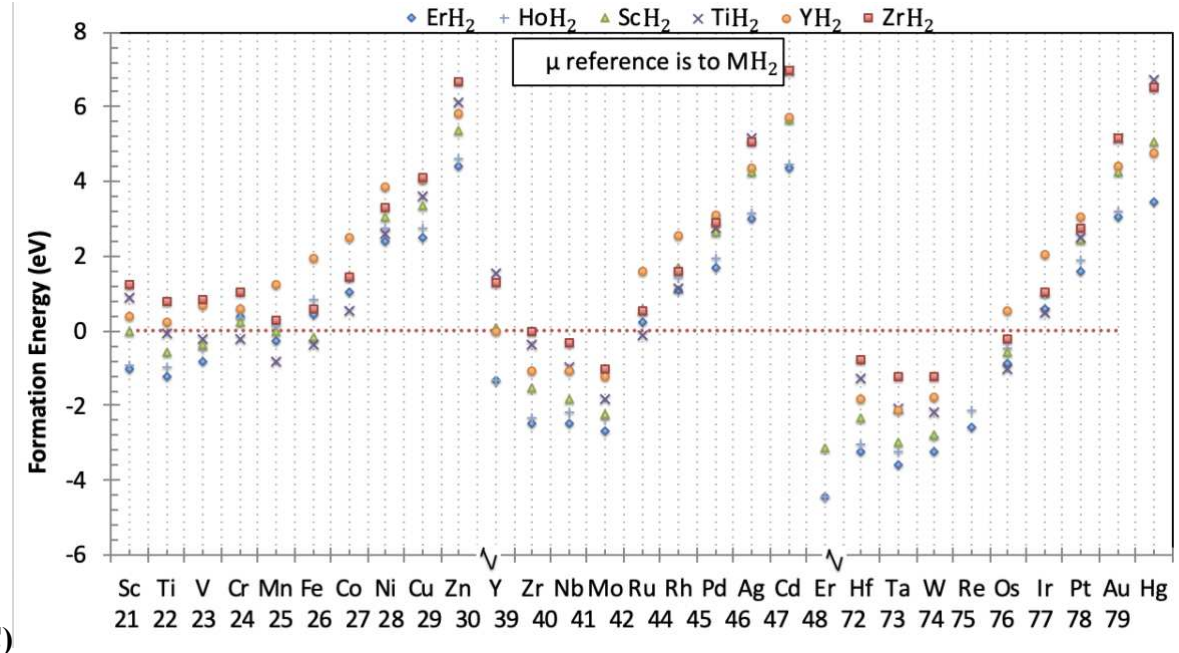

C)

Figure 4. Formation energies of substitutional defects in various metal hydrides for different reference states. A) Referenced to pure metal phase. B) Referenced to metal hydride phase. C) Referenced to metal di-hydride phase. Data is included in Section IV of the supplemental information.

B. Hydrogen Vacancy Interactions with Substitutional Dopants

The interaction of dopant atoms on the metal lattice with hydrogen vacancies was evaluated to identify if the dopants may act as sinks for hydrogen vacancies. While it is not yet understood how the migration of hydrogen vacancies impacts helium migration, it is still essential to know if these vacancies may interact with the substitutional dopants. The binding energy of a tetrahedral hydrogen vacancy to a substitutional dopant in the various metal hydrides was evaluated according to equation (**3**) and is plotted in Figure 5.

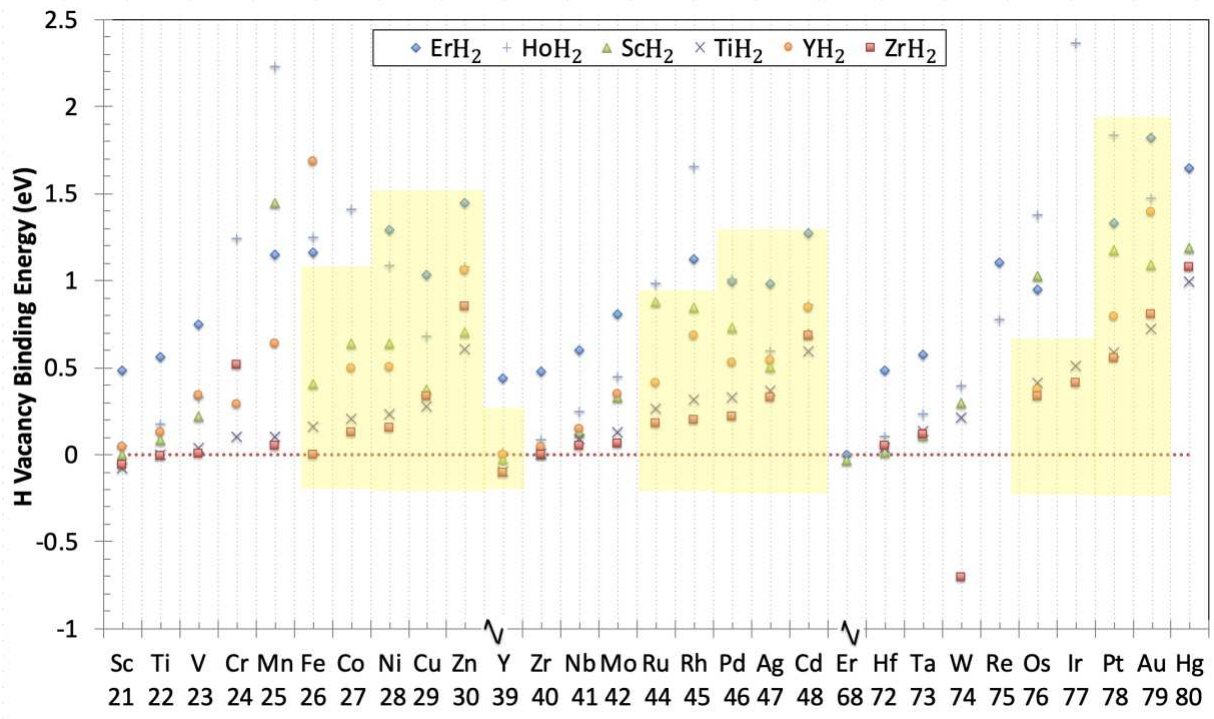

Figure 5. Binding energy of tetrahedral hydrogen vacancy to substitutional dopants in various metal hydrides. Sections shaded in yellow correspond to those elements identified in Table 3 as dopants that could be added in significant quantities. A more positive binding energy indicates a stronger binding between the dopant atom and the hydrogen vacancy. Data is included in Section IV of the supplemental information.

In general, Figure 5 shows that hydrogen vacancies tend to bind preferentially to substitutional dopants. This preferential binding indicates that the presence of these substitutional dopants may impact the mobility of hydrogen vacancies produced from the hydriding process and/or from the radioactive decay of tritium.

C. Helium Interactions with Substitutional Dopants

The interaction of helium atoms with the substitutional defects was evaluated to understand how the substitutional atoms might impact the nucleation and growth of helium bubbles. The binding

energy of an octahedral helium atom to the dopants in the various metal hydrides was evaluated according to (**4**) and is plotted in Figure 6.

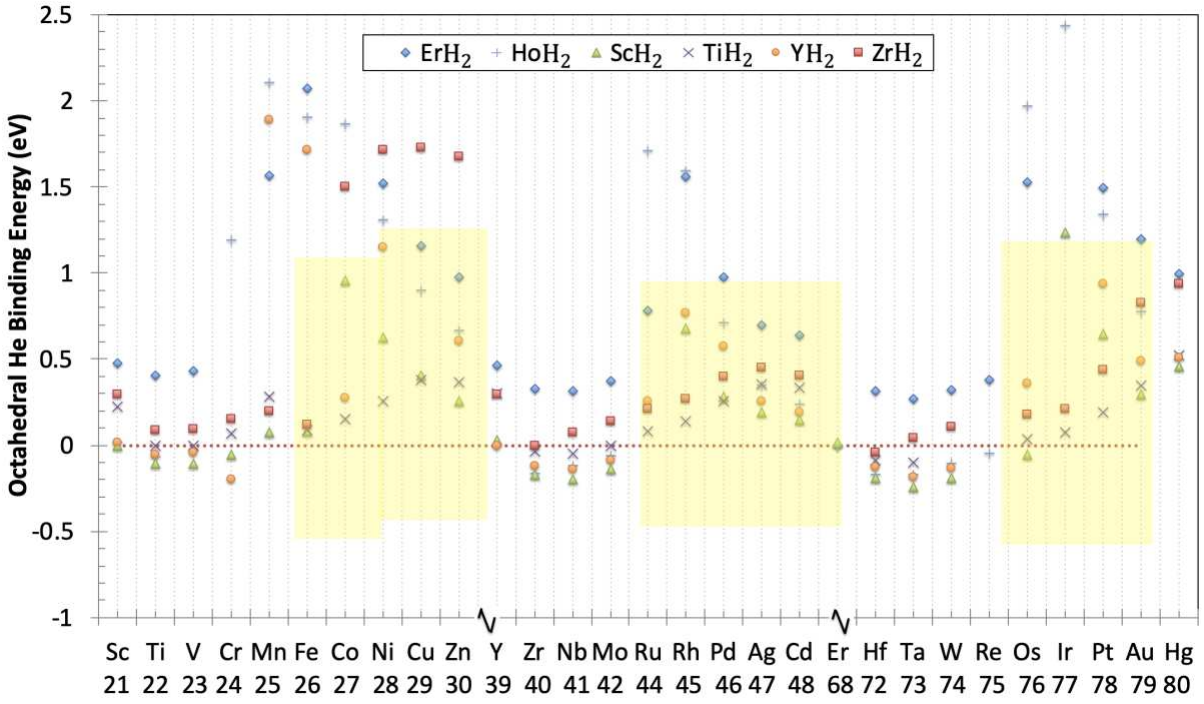

Figure 6. Binding energy of octahedral helium atoms to substitutional dopants in various metal hydrides. Sections shaded in yellow correspond to those elements identify in section 5 as dopants that could be added in relevant quantities. More positive values indicate stronger binding between the substitution and helium. Data is included in Section IV of the supplemental information.

There is a distinct pattern in the binding energies shown in Figure 6. The binding energy increases as the atom number in a given period increases, peaking around the group 8B metals and then decreasing again. Because helium is a noble gas, it is not clear why these elements would bind more tightly to helium atoms. However, analysis of the relaxed structures of the helium interstitials indicates that, in those structures with higher binding energies, the substitutional atom is displaced farther from the original matrix metal lattice site. Figure 7 shows the displacement, or distance between the initial position of the matrix metal atom and the relaxed position of the substitutional dopant, for each dopant near the helium atom in the FCC metal di-hydride. The general trend of displacement distances and binding energies for each metal hydride and dopant is summarized in Figure 8. From this plot, one can more clearly see the relationship between binding energy and displacement distance. Higher binding energies are found in structures with greater displacement between the original lattice site and the relaxed

position of the dopant atom. An example of what each of these sites looks like is shown in Figure 9. Figure 9A shows that helium pushes the substitutional atom away from the lattice position in structures with large binding energy. On the other hand, Figure 9B shows that helium does not greatly displace the substitutional atom in low binding energy structures.

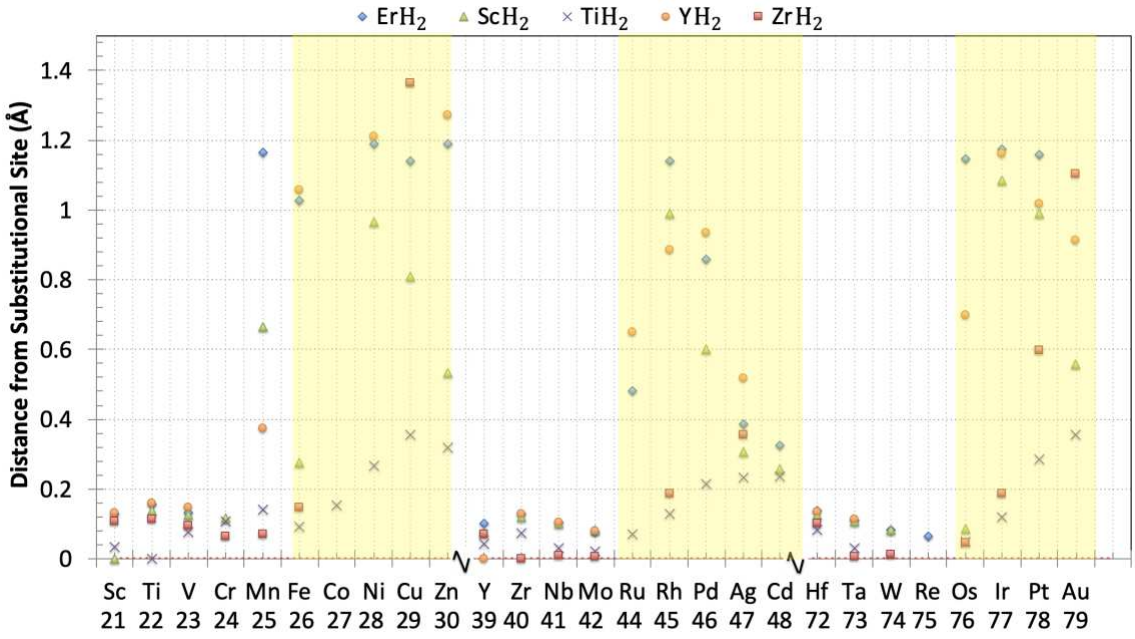

Figure 7. Displacement of dopant atom from original substitutional site near helium interstitial.

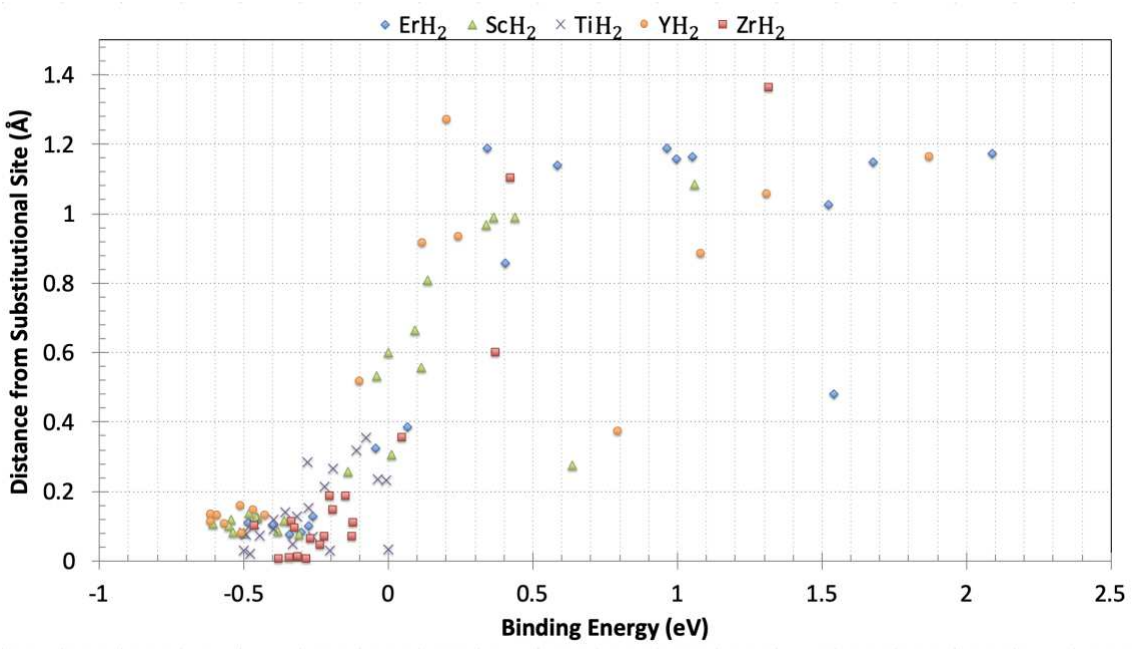

Figure 8. Binding energy vs. dopant displacement for FCC metal dihydrides.

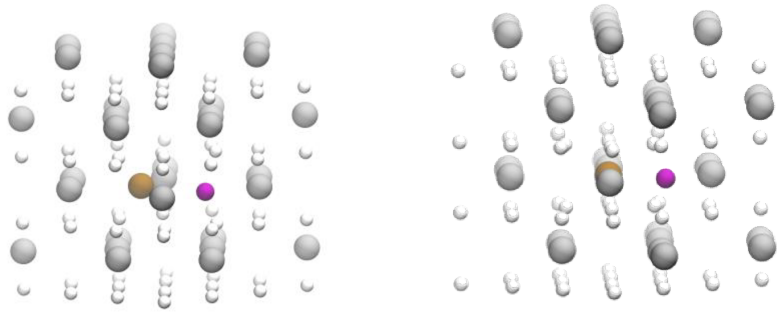

A) B)

Figure 9. Relaxed structures of helium near substitution. A) Large displacement. B) No displacement. Grey atoms represent the base metal in the metal hydride, the white atoms are hydrogen, the brown atoms are substitutional dopants and the pink atom is a helium atom.

D. Helium Substitution on Hydrogen Sub-lattice Interactions with Substitutional Dopants

Because of the prevalence of sub-stoichiometric metal hydrides and the decay of tritium, it is vital to understand how the substitutional defects interact with hydrogen vacancies and how that interaction may impact the binding energy with helium. The binding energy of the helium substitution on the hydrogen sublattice with the dopant was evaluated according to (**5**) and is shown in Figure 10.

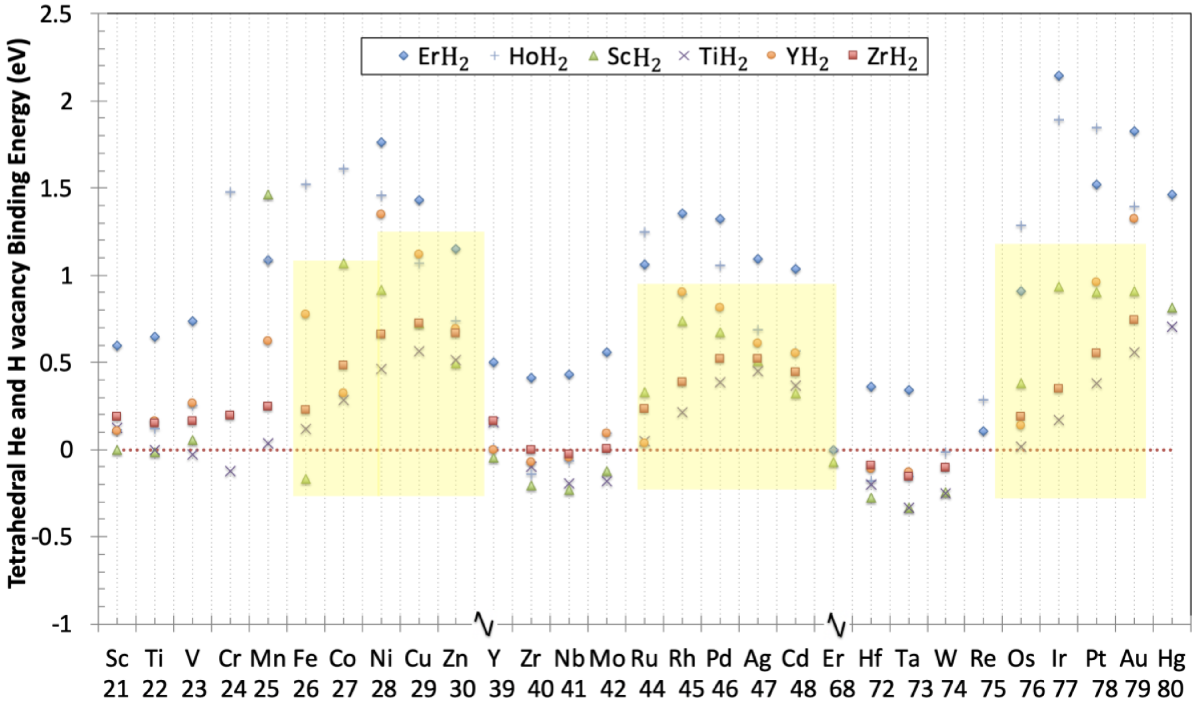

Figure 10. Binding energy of helium substitution on hydrogen sub-lattice in the tetrahedral position to dopants in various metal hydrides. Sections shaded in yellow correspond to those elements identified in Table 3 as dopants that could be added in relevant quantities. A more

positive binding energy indicates a stronger binding between the dopant atom and the hydrogen vacancy and helium interstitial. Data is included in Section IV of the supplemental information.

Figure 10 shows similar trends as those seen in the binding energy of the octahedral helium interstitials in Figure 6. Again, it is unclear why the group 8b metals show such high binding energies with the helium atoms. However, the pervasiveness of this trend may indicate that these metals could have some impact on the helium interstitial and hydrogen vacancy diffusion in these metal hydrides.

E. Analysis of Dopant Metal Solubility

Calculations of the dopant atom solubility in the metal hydride were performed to assess whether or not these substitutional dopants can be added in sufficient quantity to impact the formation and growth of helium bubbles in metal hydrides. The details of this dopant analysis are provided in the method section and covered in equations (6) through (20). After exploring a range of partial pressures of hydrogen (0.01 to 100 atm), it was found that the impact of hydrogen partial pressure on the amount of dopant atom that can be added is minimal. Therefore, only the data for the worst case (hydrogen partial pressure equal to 0.01) is shown here in Figure 11. As there are multiple possible reaction mechanisms, the reaction that resulted in the lowest tolerable amount of added dopant atoms before a competitive phase was formed was used. Therefore, the reader should keep in mind that the plots shown in Figure 11 have different reference states. Plots separated by each specific reference state are provided in section 4 of the supplemental material. The data in Figure 11 is presented as dopant atom equilibrium concentration when in contact with the dopant metal (solubility limit) as a function of temperature.

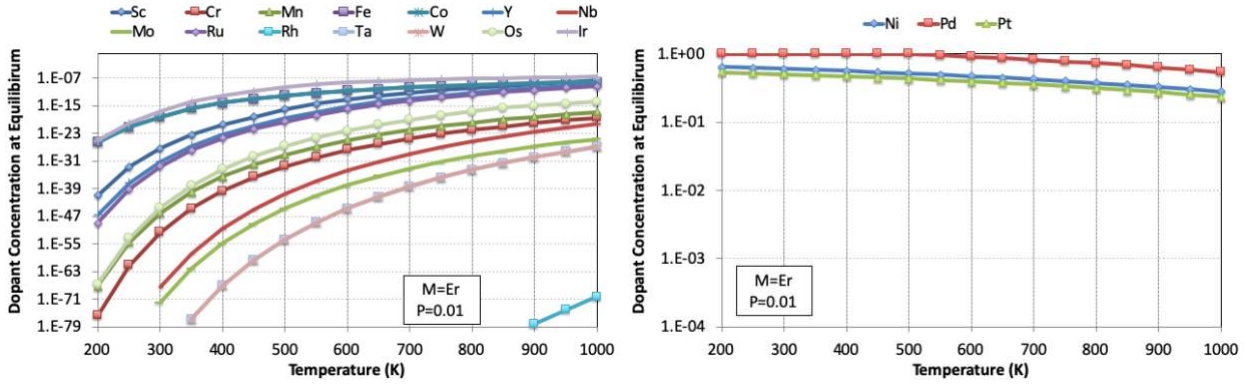

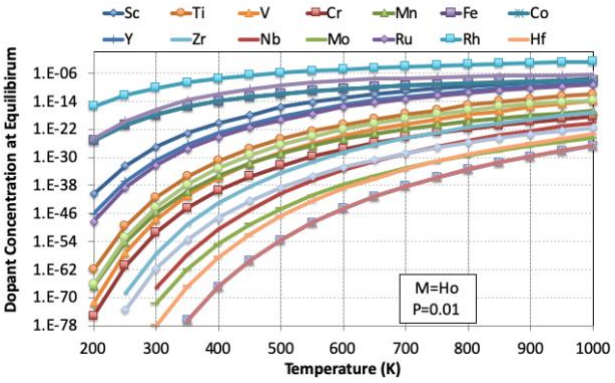
Sc Ti V Cr Mn Fe Co
Y Zr Nb Mo Ru Rh Hf
Dopant Concentration at Equilibirum
1.E-06
1.E-14
1.E-22
1.E-30
1.E-38
1.E-46
1.E-54
1.E-62
1.E-70
1.E-78
200 300 400 500 600 700 800 900 1000
Temperature (K)
M=Ho
P=0.01

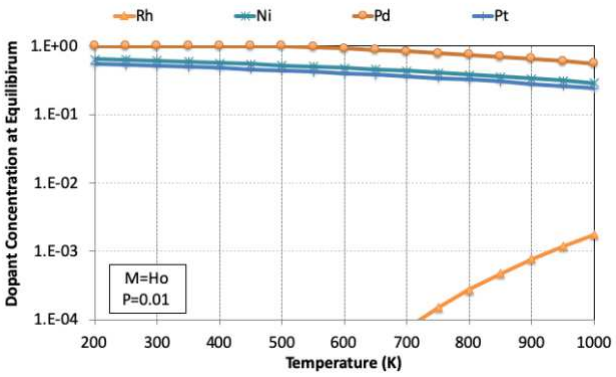
Rh Ni Pd Pt
Dopant Concentration at Equilibirum
1.E+00
1.E-01
1.E-02
1.E-03
1.E-04
200 300 400 500 600 700 800 900 1000
Temperature (K)
M=Ho
P=0.01

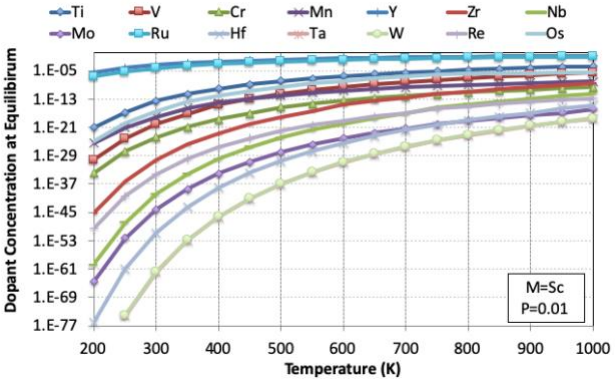
Ti V Cr Mn Y Zr Nb
Mo Ru Hf Ta W Re Os
Dopant Concentration at Equilibirum
1.E-05
1.E-13
1.E-21
1.E-29
1.E-37
1.E-45
1.E-53
1.E-61
1.E-69
1.E-77
200 300 400 500 600 700 800 900 1000
Temperature (K)
M=Sc
P=0.01

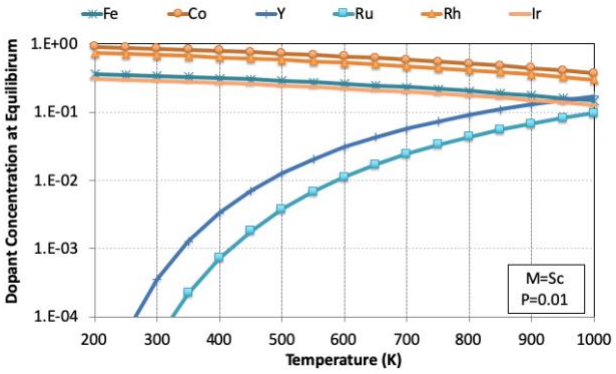
Fe Co Y Ru Rh Ir
Dopant Concentration at Equilibirum
1.E+00
1.E-01
1.E-02
1.E-03
1.E-04
200 300 400 500 600 700 800 900 1000
Temperature (K)
M=Sc
P=0.01

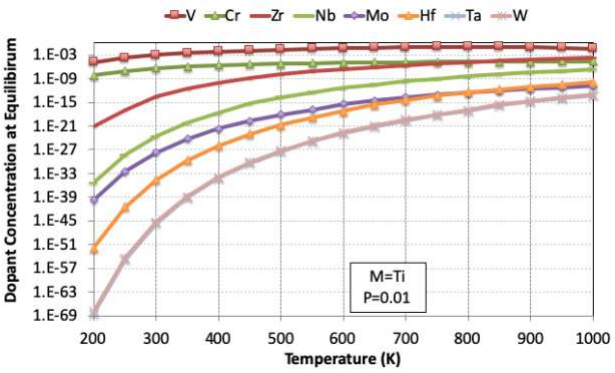
V Cr Zr Nb Mo Hf Ta W
Dopant Concentration at Equilibirum
1.E-03
1.E-09
1.E-15
1.E-21
1.E-27
1.E-33
1.E-39
1.E-45
1.E-51
1.E-57
1.E-63
1.E-69
200 300 400 500 600 700 800 900 1000
Temperature (K)
M=Ti
P=0.01

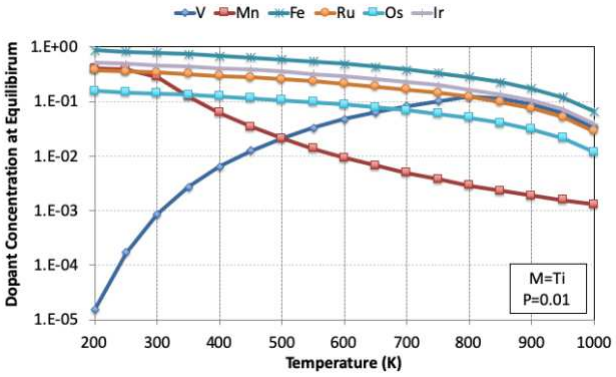
V Mn Fe Ru Os Ir
Dopant Concentration at Equilibirum
1.E+00
1.E-01
1.E-02
1.E-03
1.E-04
1.E-05
200 300 400 500 600 700 800 900 1000
Temperature (K)
M=Ti
P=0.01

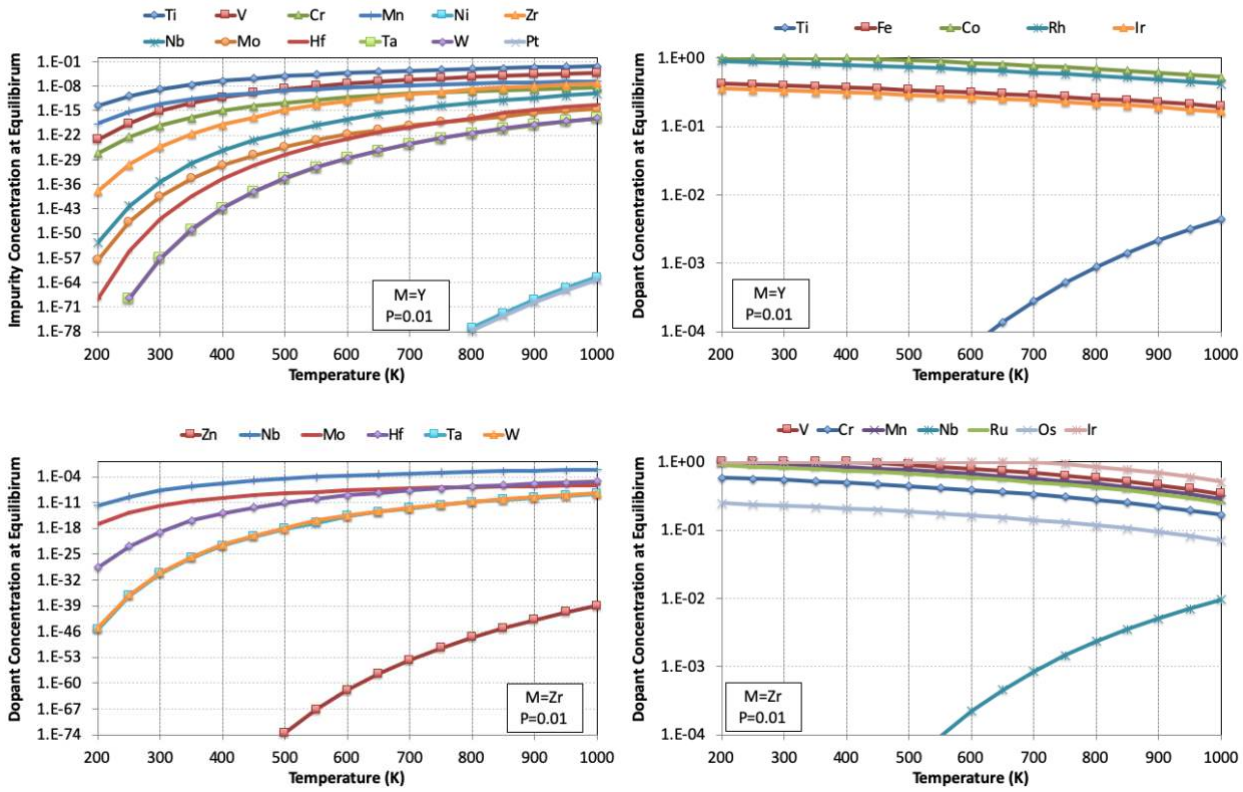

Figure 11. Maximum concentration of dopants at a given temperature and pressure for various metal hydrides. Data for calculating these values at various pressures and temperatures is included in Section IV of the supplemental information.

It can be seen from the plots in Figure 11 that only small amounts of dopant atoms can be added to the metal hydrides without causing the formation of competing phases. This is especially true for the rare-earth metal hydrides ErH_2 and HoH_2, whereas the transition metal hydrides TiH_2 and ZrH_2 allowed for several different dopant atoms to be added in much larger quantities. The competing dopant di-hydride (DH_2) phase was determined to have the most significant impact on the dopant solubility. While this phase is often unstable for many dopants, it would indicate that other intermetallic phases not considered here could be more stable than the dopant phase. Experimental investigations of helium in metal hydrides often have helium bubble densities between $1x10^{17}$ bubbles/cm^3 and $1x10^{19}$ bubbles/cm^3 [40] or between $1x10^{-6}$ bubbles/base metal atom and $1x10^{-4}$ bubbles/base metal atom. Therefore, for a dopant to meaningfully impact the helium bubble density, it must be able to be added to the metal hydride in concentrations of greater than $1x10^{-3}$ dopant atom/base metal atom to exceed the naturally occurring densities. Smaller concentrations of dopant atoms may still be impactful, but here we chose to focus on those with the most potential impact on bubble densities. Table 3 lists those dopant elements

that could be added above this cutoff value for a wide variety of temperatures for each metal hydride.

Table 3. Relevant dopant elements by metal hydride

Metal Hydride	Relevant stable dopant elements
ErH_2	Ni, Cu, Zn, Pd, Ag, Cd, Pt, Au
HoH_2	Ni, Cu, Zn, Pd, Ag, Cd, Pt, Au
ScH_2	Fe, Co, Ni, Cu, Zn, Y, Ru, Rh, Pd, Ag, Cd, Ir, Pt, Au
TiH_2	Sc, V, Mn, Fe, Co, Ni, Cu, Zn, Y, Ru, Rh, Pd, Ag, Cd, Os, Ir, Pt, Au
YH_2	Sc, Fe, Co, Cu, Zn, Rh, Pd, Ag, Cd, Ir, Au
ZrH_2	Sc, Ti, V, Cr, Mn, Fe, Co, Ni, Cu, Y, Ru, Rh, Pd, Ag, Cd, Os, Ir, Pt, Au

4. Discussion

Based on the data in figures 6, 7, and 11, almost all of the elements listed in Table 3 that can be added in sufficient quantities to impact the nucleation density will have positive binding energy to helium interstitials and hydrogen vacancies. Assuming this binding energy relationship holds for an increasing amount of helium, these dopants may impact the overall helium bubble density in these metal hydrides.

Cowgill developed an analytical model based on continuum mechanics of the time to fracture of a palladium hydride based on helium bubble growth (see [41] for details on this model and its use). The model assumes isotropic material properties and a random but homogeneous distribution of spherical bubbles. It assumes a helium diffusion constant based on experimental data, a Burgers vector length, surface energy, shear modulus, and fracture strength based on the properties of PdH_X. While these properties may vary between the metal hydrides considered in this study and the palladium hydride considered by Cowgill, it is possible to relate changes in helium bubble density to estimated times of fracture for a metal hydride film using this analytical model. While the model makes a few simplifying assumptions that may or may not be applicable for the metal hydrides considered here, it is expected to allow approximate trends to be identified. Figure 12 shows the relationship as predicted by the Cowgill model between bubble density and time to fracture based on various temperatures, surface energies, and fracture

strengths. The distribution of surface energies and fracture strengths covers a range of properties relevant to the metal hydrides previously discussed. As these properties can depend on the specifics of a system, these plots serve as a general guide for experimentalists. The model tends to indicate that there is an optimal bubble density for maximizing the time to fracture of a given metal hydride film. Based on the results shown in the previous section, it may be possible to use dopant metals to alter the bubble density to maximize the time to fracture for a specific system.

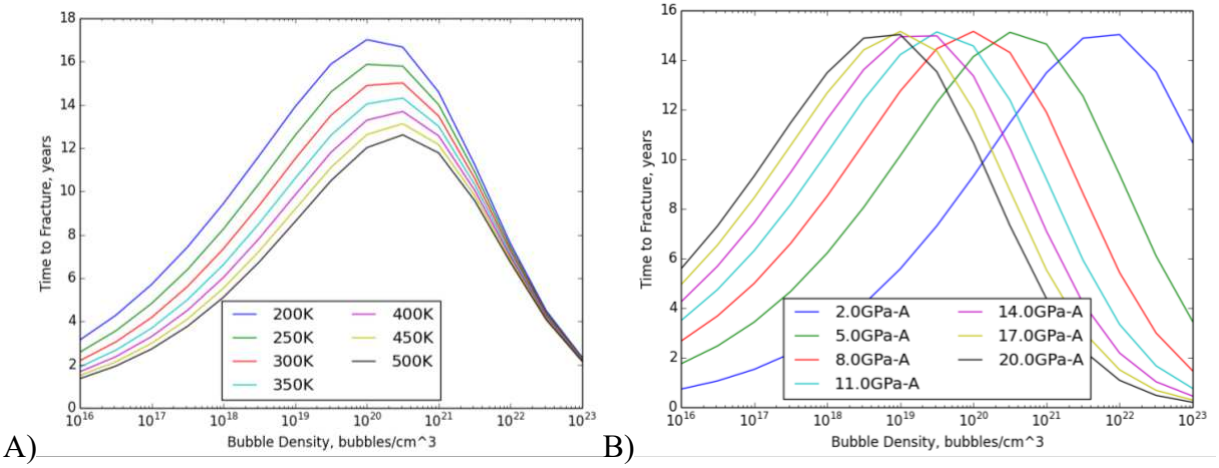

A) B)

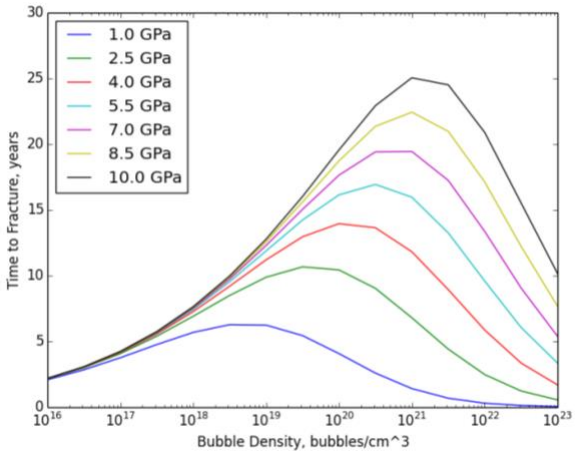

C)

Figure 12. Cowgill model predictions for relationship between helium bubble density and time to fracture for different (A) Temperatures, (B) Metal hydride surface energies, and (C) Metal hydride Fracture strength. See [41] for details on this model and its use.

5. Concluding Remarks

The impact of transition metal substitutional dopants in FCC rare earth and transition metal hydrides on the interaction with helium was investigated using density functional theory. Thermodynamic calculations were conducted to identify which transition metals could be added in sufficient quantity to impact helium bubble density but not result in the formation of

competing phases that may reduce the amount of hydrogen that can be stably stored in the metal hydrides. Many of the transition metals could not be added to the rare earth metal hydrides (ErH_2 and HoH_2) in a sufficient quantity before competing phases would form. However, the transition metal hydrides, in particular TiH_2 and ZrH_2, allowed for the possibility of more substantial quantities of dopant metals to be added without forming competing hydride phases. It was found that several of these dopants metals resulted in an increase in the hydrogen vacancy, helium interstitial, and combined interstitial and vacancy binding energies. In particular, those elements in the 8b group of the periodic table displayed the most preferential binding with the helium interstitials and hydrogen vacancies. It was found that these metals also exhibited the largest amount of displacement from the substitutional metal site compared to those with lower binding energies. While the mechanism for this increased binding energy for these metals is still unclear, it suggests that manipulating the helium bubble density in metal hydrides may be possible using these dopant metals. Experimental studies of these metals are necessary to evaluate the impact on helium bubble characteristics and explore the effects of potential competing intermetallic phases that may form depending on the hydriding conditions. Using analytical models, altering the helium bubble density may increase the time to fracture of a metal hydride system increasing the potential tritium storage time of these metal hydrides.

Acknowledgments

Sandia National Laboratories is a multi-mission laboratory managed and operated by National Technology and Engineering Solutions of Sandia, LLC., a wholly owned subsidiary of Honeywell International, Inc., for the U.S. Department of Energy's National Nuclear Security Administration under contract DE-NA0003525. This paper describes objective technical results and analysis. Any subjective views or opinions that might be expressed in the paper do not necessarily represent the views of the U.S. Department of Energy or the United States Government. Support for D. M. was provided by the National Science Foundation Cyberinfrastructure for Sustained Scientific Innovation (CSSI) program, award No. 1931298.

References

[1] P. van der Sluis, M. Ouwerkerk, and P. A. Duine, "Optical switches based on magnesium lanthanide alloy hydrides," *Appl. Phys. Lett.*, vol. 70, no. 25, p. 3356, 1997.
[2] J. N. Huiberts *et al.*, "Yttrium and lanthanum hydride films with switchable optical properties," *Nature*, vol. 380, no. 6571, pp. 231–234, Mar. 1996.
[3] P. H. Notten, "Electrochromic metal hydrides," *Curr. Opin. Solid State Mater. Sci.*, vol. 4, no. 1, pp. 5–10, Feb. 1999.
[4] R. Griessen, "Schaltbare Spiegel aus Metallhydriden," *Phys. J.*, vol. 53, no. 12, pp. 1207–

1209, Dec. 1997.
[5] C. Christofides and A. Mandelis, “Solid-state sensors for trace hydrogen gas detection,” *J. Appl. Phys.*, vol. 68, no. 6, p. R1, 1990.
[6] B. Hjörvarsson, C. Chacon, H. Zabel, and V. Leiner, “Adjustable magnetic interactions: the use of hydrogen as a tuning agent,” *J. Alloys Compd.*, vol. 356–357, pp. 160–168, Aug. 2003.
[7] K. Yoshimura, C. Langhammer, and B. Dam, “Metal hydrides for smart window and sensor applications,” *MRS Bull.*, vol. 38, no. 06, pp. 495–503, Jun. 2013.
[8] B. Sakintuna, F. Lamaridarkrim, and M. Hirscher, “Metal hydride materials for solid hydrogen storage: A review☆,” *Int. J. Hydrog. Energy*, vol. 32, no. 9, pp. 1121–1140, Jun. 2007.
[9] P. Jena, “Materials for Hydrogen Storage: Past, Present, and Future,” *J. Phys. Chem. Lett.*, vol. 2, no. 3, pp. 206–211, Feb. 2011.
[10] M. Conte, P. Prosini, and S. Passerini, “Overview of energy/hydrogen storage: state-of-the-art of the technologies and prospects for nanomaterials,” *Mater. Sci. Eng. B*, vol. 108, no. 1–2, pp. 2–8, Apr. 2004.
[11] A. Baldi and B. Dam, “Thin film metal hydrides for hydrogen storage applications,” *J Mater Chem*, vol. 21, no. 12, pp. 4021–4026, 2011.
[12] A. Zaluska, L. Zaluski, and J. O. Ström-Olsen, “Structure, catalysis and atomic reactions on the nano-scale: a systematic approach to metal hydrides for hydrogen storage,” *Appl. Phys. Mater. Sci. Process.*, vol. 72, no. 2, pp. 157–165, Feb. 2001.
[13] N. Park, K. Choi, J. Hwang, D. W. Kim, D. O. Kim, and J. Ihm, “Progress on first-principles-based materials design for hydrogen storage,” *Proc. Natl. Acad. Sci.*, vol. 109, no. 49, pp. 19893–19899, Dec. 2012.
[14] P. A. Schultz and C. S. Snow, “Mechanical properties of metal dihydrides,” *Model. Simul. Mater. Sci. Eng.*, vol. 24, no. 3, p. 035005, Mar. 2016.
[15] R. P. Gupta and M. Gupta, “Consequences of helium production from the radioactive decay of tritium on the properties of palladium tritide,” *Phys. Rev. B*, vol. 66, no. 1, Jul. 2002.
[16] NATO Advanced Research Workshop on Fundamental Aspects of Inert Gases in Solids, S. E. Donnelly, J. H. Evans, North Atlantic Treaty Organization, and Scientific Affairs Division, *Fundamental aspects of inert gases in solids*. 1991.
[17] X. Xiang, C. A. Chen, K. Z. Liu, L. X. Peng, and Y. C. Rao, “Effect of Fe and C doping on the thermal release of helium from aluminum,” *Fusion Eng. Des.*, vol. 85, no. 10–12, pp. 2086–2089, Dec. 2010.
[18] J. Zhang, E. Wu, and S. Liu, “Effects of Y on helium behavior in Ti–Y alloy films,” *J. Nucl. Mater.*, vol. 454, no. 1–3, pp. 119–125, Nov. 2014.
[19] M. K. Matta and W. Kesternich, “Microstructure and thermomechanical pretreatment effects on creep behaviour of helium-implanted DIN 1·4970 austenitic stainless steel,” *Bull. Mater. Sci.*, vol. 13, no. 5, pp. 313–322, 1990.
[20] W. Hao and W. T. Geng, “Gold might slow down the growth of helium bubble in iron,” *Nucl. Instrum. Methods Phys. Res. Sect. B Beam Interact. Mater. At.*, vol. 269, no. 12, pp. 1428–1430, Jun. 2011.
[21] W. Hao and W. T. Geng, “Impeding effect of Ce on He bubble growth in bcc Fe,” *Nucl. Instrum. Methods Phys. Res. Sect. B Beam Interact. Mater. At.*, vol. 280, pp. 22–25, Jun. 2012.
[22] G. Kresse and J. Furthmüller, “Efficient iterative schemes for *ab initio* total-energy calculations using a plane-wave basis set,” *Phys. Rev. B*, vol. 54, no. 16, pp. 11169–11186, Oct. 1996.
[23] J. P. Perdew, K. Burke, and M. Ernzerhof, “Generalized Gradient Approximation Made

Simple," *Phys. Rev. Lett.*, vol. 77, no. 18, pp. 3865–3868, Oct. 1996.
[24] Kresse, G. and Joubert, D., "From ultrasoft pseudopotentials to the projector augmented-wave method," *Phys. Rev. B*, vol. 59, no. 3–15, pp. 1758–1775, Jan. 1999.
[25] F. Ducastelle, R. Caudron, and P. Costa, "Propriétés électroniques des hydrures des systèmes Ti-H et Zr-H," *J. Phys.*, vol. 31, no. 1, pp. 57–64, 1970.
[26] Walter Wolf and Peter Herzig, "First-principles investigations of transition metal dihydrides, TH 2 : T = Sc, Ti, V, Y, Zr, Nb; energetics and chemical bonding," *J. Phys. Condens. Matter*, vol. 12, no. 21, p. 4535, 2000.
[27] J. A. Grimshaw, F. J. Spooner, C. G. Wilson, and A. D. McQuillan, "The growth of crystals of erbium hydride," *J. Mater. Sci.*, vol. 16, no. 10, pp. 2855–2859, 1981.
[28] A. Pebler and W. E. Wallace, "CRYSTAL STRUCTURES OF SOME LANTHANIDE HYDRIDES [1]," *J. Phys. Chem.*, vol. 66, no. 1, pp. 148–151, Jan. 1962.
[29] Y. Khodyrev and R. V. Baranova, *Kristallografiya*, vol. 25, p. 172, 1980.
[30] H. L. Yakel, "Thermocrystallography of higher hydrides of titanium and zirconium," *Acta Crystallogr.*, vol. 11, no. 1, pp. 46–51, Jan. 1958.
[31] J. N. Daou and P. Vajda, "Hydrogen ordering and metal-semiconductor transitions in the system YH 2 + x," *Phys. Rev. B*, vol. 45, no. 19, pp. 10907–10913, May 1992.
[32] K. Niedźwiedź, B. Nowak, and O. J. żogał, "91Zr NMR in non-stoichiometric zirconium hydrides, ZrHx ($1.55 \leqslant x \leqslant 2$)," *J. Alloys Compd.*, vol. 194, no. 1, pp. 47–51, Apr. 1993.
[33] T. Mayeshiba *et al.*, "The MAterials Simulation Toolkit (MAST) for atomistic modeling of defects and diffusion," *Comput. Mater. Sci.*, vol. 126, pp. 90–102, Jan. 2017.
[34] R. R. Wixom, J. F. Browning, C. S. Snow, P. A. Schultz, and D. R. Jennison, "First principles site occupation and migration of hydrogen, helium, and oxygen in β-phase erbium hydride," *J. Appl. Phys.*, vol. 103, no. 12, p. 123708, 2008.
[35] J. H. Liang *et al.*, "Ab initio study of helium behavior in titanium tritides," *Comput. Mater. Sci.*, vol. 69, pp. 107–112, Mar. 2013.
[36] R.-C. Chen *et al.*, "*Ab initio* study of H and He migrations in β-phase Sc, Y, and Er hydrides," *Chin. Phys. B*, vol. 21, no. 5, p. 056601, May 2012.
[37] T. Angsten, T. Mayeshiba, H. Wu, and D. Morgan, "Elemental vacancy diffusion database from high-throughput first-principles calculations for fcc and hcp structures," *New J. Phys.*, vol. 16, no. 1, p. 015018, Jan. 2014.
[38] Natacha Bourgeois, Jean-Claude Crivello, Pierre Cenedese, Valerie Paul-Boncour, and Jean-Marc Joubert, "Vibration analysis of hydrogen, deuterium and tritium in metals: consequences on the isotope effect," *J. Phys. Condens. Matter*, vol. 30, p. 335402, Jun. 2018.
[39] M. W. Chase, "NIST-JANAF Themochemical Tables," *J. Phys. Chem. Ref. Data*, vol. 9, no. 4, pp. 1–1951, 1998.
[40] G. M. Bond, J. F. Browning, and C. S. Snow, "Development of bubble microstructure in ErT2 films during aging," *J. Appl. Phys.*, vol. 107, no. 8, p. 083514, 2010.
[41] D. F. Cowgill, "Physics of He Platelets in Metal Tritides," *Eff. Hydrog. Mater.*, p. 686, 2008.